JCIM JOURNAL OF CHEMICAL INFORMATION AND MODELING

pubs.acs.org/jcim Article

Separation Selectivity of CH_4/CO_2 Gas Mixtures in the ZIF-8 Membrane Explored by Dynamic Monte Carlo Simulations

Zheng Wan,[⊥] Guobing Zhou,[⊥] Zhongyang Dai, Li Li, Na Hu, Xiangshu Chen,* and Zhen Yang*

Cite This: *J. Chem. Inf. Model.* 2020, 60, 2208−2218 Read Online

ACCESS | Metrics & More | Article Recommendations | Supporting Information

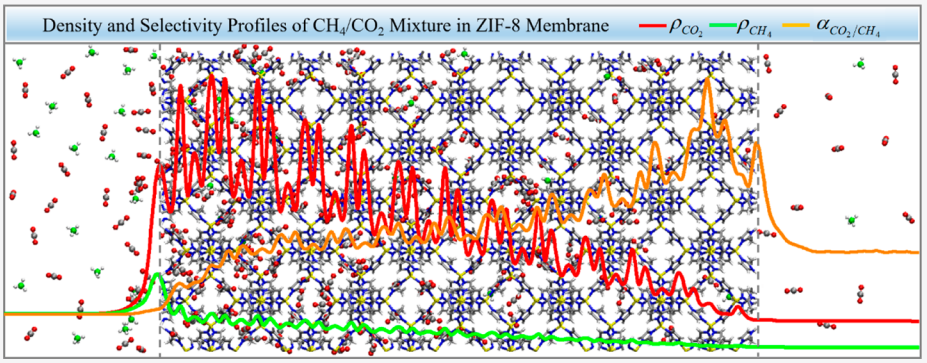

ABSTRACT: Here we report a series of nonequilibrium dynamic Monte Carlo simulations combined with dual control volume (DCV-DMC) to explore the separation selectivity of CH_4/CO_2 gas mixtures in the ZIF-8 membrane with a thickness of up to about 20 nm. Meanwhile, an improved DCV-DMC approach coupled with the corresponding potential map (PM-DCV-DMC) is further developed to speed up the computational efficiency of conventional DCV-DMC simulations. Our simulation results provide the molecular-level density and selectivity profiles along the permeation direction of both CH_4 and CO_2 molecules in the ZIF-8 membrane, indicating that the parts near membrane surfaces at both ends play a key role in determining the separation selectivity. All densities initially show a sharp increase in the individual maximum within the first outermost unit cell at the feed side and follow a long fluctuating decrease process. Accordingly, the corresponding selectivity profiles initially display a long fluctuating increase in the individual maximum and follow a sharp decrease near the membrane surface at the permeation side. Furthermore, the effects of feed composition, temperature, and pressure on the relevant separation selectivity are also discussed in detail, where the temperature has a greater influence on the separation selectivity than the feed composition and pressure. More importantly, the predicted separation selectivities from our PM-DCV-DMC simulations are well consistent with previous experimental results.

1. INTRODUCTION

Zeolitic imidazolate frameworks (ZIFs), as a novel subfamily of metal organic frameworks (MOFs),[1−4] have been considered as one of the most fascinating nanoporous materials for various applications.[5−7] Among these, gas storage and separation in ZIFs have received tremendous attention in the past decades not only because of their highly porous framework, large accessible surface area, and suitable pore apertures but also because of their exceptional chemical and thermal stabilities in both aqueous and organic media compared to other MOFs.[8−11] Based on such superior intrinsic properties, furthermore, the ZIFs have been widely applied as the membrane materials for different gas separations[12−14] since the pioneer work of the ZIF-8 membrane proposed by Caro and co-workers[15] in 2009. Subsequently, considerable efforts have been devoted to the synthesis of various ZIF-based membranes, including ZIF-7,[16−18] ZIF-8,[15,19−30] ZIF-9,[31] ZIF-11,[32] ZIF-22,[33] ZIF-67,[34] ZIF-69,[35] ZIF-71,[36,37] ZIF-78,[38] ZIF-90,[39−41] ZIF-93,[42] ZIF-95,[43,44] and ZIF-100.[44] Nevertheless, the relevant knowledge of the separation mechanism of gas mixtures in ZIF-based membranes is still rather lacking up to now, which significantly hinders the practical preparation and application of ZIF-based membranes with tailored properties. Therefore, it is extremely critical to provide a microscopic understanding of the relevant separation mechanism of gas mixtures in ZIF-based membranes.

As a powerful analysis tool, molecular simulations, including molecular dynamics (MD) and Monte Carlo (MC) methods, can provide molecular-level insight into the adsorption, diffusion, and separation behaviors of gas mixtures inside various microporous materials and their membrane materi-

Received: January 30, 2020
Published: March 25, 2020

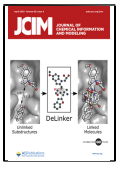

als.[45−54] For example, Sholl and co-workers[50] have successfully developed an efficient computational model by introducing a geometric method, which can not only quickly identify the key features of the pore structure but also combine molecular simulation calculations to predict the Henry's constant for adsorption and diffusion activation energy of spherical adsorbates, to evaluate a larger number of MOFs (>500) and silica zeolites (>160) for kinetic separations of simple gases including CO_2, CH_4, and H_2. Krishna and van Baten[51] used configurational-bias MC and MD simulations to examine the adsorption, diffusion, and permeation selectivities for the separation of CO_2/H_2, CH_4/CO_2, CO_2/N_2, CH_4/N_2, and CH_4/H_2 mixtures in a wide variety of zeolites and their membranes. Snurr and co-workers[52] used the conventional grand canonical MC method to rapidly screen 137,953 hypothetical MOFs by calculating each of their pore-size distribution, surface area, and methane-storage capacity. Such larger-scale screening predicted more than 300 MOFs with a predicted methane-storage capacity better than that of any known material at that time, where one of the promising MOFs with methyl functional groups was experimentally synthesized and confirmed its predicted capacity. Although a number of previous molecular modeling calculations have shown their powerful abilities to screen the possible microporous materials and their membranes, these equilibrium molecular modelings are only able to provide an indirect prediction for the permeation selectivity of membranes in terms of the product of the adsorption selectivity and the diffusion selectivity. Such indirect calculations based on equilibrium molecular modelings are possibly reasonable only when the membranes are thick enough to ignore the contribution of surface resistances so that the intracrystalline resistances dominate the overall mass transfer across the membrane.[55−59]

However, the real thicknesses of the high-performance membranes are often less than 1 μm, which are not thick enough to ignore the surface resistances. Therefore, it is necessary to employ nonequilibrium molecular modelings to explore the real separation processes of gas mixtures in various membranes. Currently, there are two kinds of nonequilibrium molecular modelings used to study the membrane separation behavior of gas mixtures. One is based on the MD algorithm (denoted as the nonequilibrium MD algorithm) through solving the Newton's equation of motion to generate the motions of particles,[60−68] where the dual control volume grand canonical MD (DCV-GCMD) method is the most widely used.[60−65] For example, Xu et al.[61] used the DCV-GCMD method for the first time to study the transport behavior of CH_4/CO_2 mixtures in carbon nanopore with the presence of a realistic external chemical potential gradient. Sahimi and co-workers[62,63,69] performed a series of DCV-GCMD simulations to explore the transport and separation processes of H_2/CO_2 and H_2/CH_4 mixtures in their atomistic model of amorphous SiC membranes with the thickness of up to 38.52 nm. They found that both the temperature and the membrane thickness have a significant influence on the separation factor, but the pressure drop across the membrane almost has no effect.[63] More recently, a novel concentration gradient driven MD (CGD-MD) proposed by Ozcan and co-workers,[68] where a bias force was introduced to fix the concentration of fluids at target values at the inlet and outlet of a membrane, was successfully used to study the permeation of pure CH_4, C_2H_4, and C_2H_6, as well as the separation of equimolar C_2H_4/C_2H_6 through the ZIF-8 membrane with the thickness of 8.5 nm. Their calculated C_2H_4/C_2H_6 selectivity is well consistent with the experimental data. Although these nonequilibrium MD algorithms are able to theoretically produce the most realistic processes of membrane separations, they are extremely time-consuming since gas molecules often diffuse very slowly through a membrane. Therefore, most of the previous nonequilibrium MD simulations were carried out with thin membranes, low fluid densities, and high temperatures, which are favorable to the motions of molecules in membranes. Even so, there are still a small number of gas molecules across the very thin membranes after a long-time simulation, failing to attain reliable simulation results.

On the other hand, the other nonequilibrium molecular modeling based on the MC algorithm (denoted as the nonequilibrium MC algorithm) to produce motions of particles, mainly including kinetic MC (KMC)[70] or also called dynamic MC (DMC)[71,72] and DMC combined with dual control volume (DCV-DMC)[73−75] and also called dual ensemble MC (DEMC),[76] was also widely used to study the permeation and separation of molecules or ions in different membranes. In principle, the developed DMC algorithm can be used to simulate the dynamics of the system, which is actually based on the interpretation of a Markov chain as the evolution of the system in time, and every type of displacement of particles in the system has its own frequency reflecting the number of events per unit time.[73,75] Although the DCV-DMC simulation does not produce exact trajectories, it reproduces dynamical properties on average. For example, very early DCV-DMC simulations of Seo et al.[73] demonstrated the transport diffusion of H_2, CH_4, C_2H_6, C_3H_8, and n-C_4H_{10} in nanoporous carbon membranes with slitlike pores, where their relative fluxes are in semiquantitative agreement with the relevant experimental data. Rutkai et al.[74] further extended the DCV-DMC simulation to explore the dynamical selectivity of Ca^{2+} and Na^+ in a model calcium channel with the stronger binding affinity between the ions and the calcium channel. Despite great progress, it should be noted that such a DMC algorithm does not provide an absolute measure of real time but does give the relative rates of dynamic processes.[72,77] However, the nonequilibrium MC algorithm is used at least reasonably to explore the selectivity other than flux of molecules and ions in membranes.[73−75,77] Compared to the nonequilibrium MD algorithms, furthermore, the advantages of nonequilibrium MC algorithms are more considerable when the membrane is thick, the density in the pore is high, the temperature is low, or the fluid particles interact strongly with the pore wall, since the fundamental MC algorithm to make nonphysical moves can significantly enhance its capacity to explore phase space especially when the fluid particles are simple gas molecules or ions.

In the present work, a series of DCV-DMC simulations in combination with the corresponding potential maps[78,79] (denoted as the PM-DCV-DMC simulation) were conducted to explore the separation selectivity of CH_4/CO_2 gas mixtures in the ZIF-8 membrane with a thickness of up to about 20 nm, as described by the experiments of Venna and Carreon.[21] Herein, we have adjusted the force field between gas molecules and the ZIF-8 framework to better reproduce the experimental adsorption data. Further, we have compared the simulation results between the improved PM-DCV-DMC and the original DCV-DMC simulations to test the validity of the improved method. Based on the adjusted force field and the improved

https://dx.doi.org/10.1021/acs.jcim.0c00114
J. Chem. Inf. Model. 2020, 60, 2208−2218

PM-DCV-DMC method, then, we have focused on the effects of the feed composition, pressure drop, and temperature on the density gradient profiles and separation selectivities of CH_4/CO_2 mixtures in the ZIF-8 membrane. More importantly, our simulation results are well consistent with the experimental separation selectivities of CH_4/CO_2 mixtures in the ZIF-8 membrane. The rest of this paper is organized as follows. In section 2, we describe the details of both the force field and the improved PM-DCV-DMC simulation. In Section 3, we present the simulation results for the density gradient profiles along the permeation direction of CO_2 and CH_4 in the ZIF-8 membrane as well as the corresponding separation selectivities under different conditions. Finally, several brief conclusions are summarized in Section 4.

2. SIMULATION DETAILS

2.1. Potential Model. In this work, the crystal structure of the ZIF-8 membrane for the PM-DCV-DMC simulations was constructed by duplicating 3 × 3 × 12 unit cells in *x*, *y*, and *z* directions in terms of the experimental X-ray diffraction data of the Cambridge Structural Database. Accordingly, the dimensions of the ZIF-8 membrane are 5.1 × 5.1 × 20.4 nm^3. The periodic boundary condition was only applied in both *x* and *y* directions, while the N atoms of imidazolium rings on the membrane surfaces perpendicular to the *z* direction were saturated by the H atoms. For the reason for computational economy, an uncharged single-point model was used for both the CH_4 and CO_2 molecules, the whole ZIF-8 membrane was always rigid in the following PM-DCV-DMC simulations, and its potential model used here was from the force field proposed by Zheng et al.[80] Based on the above force fields, the nonbonded interactions were described only by the Lennard-Jones (L-J) interactions and the crossing L-J parameters were derived for self-parameters using the Lorenz-Berthelot mixing rule.

To further test the validity of our potential model used in this work, a series of grand canonical MC (GCMC) simulations were carried out for the adsorption isotherms at 298 K of pure CH_4 and CO_2 molecules in ZIF-8, respectively. By comparison with the experimental data reported by Venna et al.,[21] the GCMC simulations based on the original potential model obviously overestimated the adsorption amounts of CH_4 molecules in ZIF-8 but underestimated those of CO_2 molecules, as shown in Figure 1. In order to improve the accuracy of our potential model, we introduced different empirical parameters to scale the energy parameters ε of CH_4 and CO_2 molecules, where the scaling parameters are 1.015 and 0.66 for the CH_4 and CO_2 molecules, respectively. Then, Figure 1 clearly indicates that the simulation results with the adjusted potential model are well consistent with the experimental adsorption data. Therefore, we employed the improved potential model in the following PM-DCV-DMC simulations, and all L-J parameters used in this work were summarized in Table 1.

2.2. Details of PM-DCV-DMC Simulation. In general, there are three main steps for the whole separation process of gas molecules in the membrane: 1) adsorption of gas molecules from the feed phase to the membrane surface; 2) permeation of the adsorbed gas molecules through the membrane; and 3) desorption of gas molecules from the membrane surface to the permeation phase. In this work, we employed the PM-DCV-DMC method to simulate such a realistic separation process. It is worth noting that the original

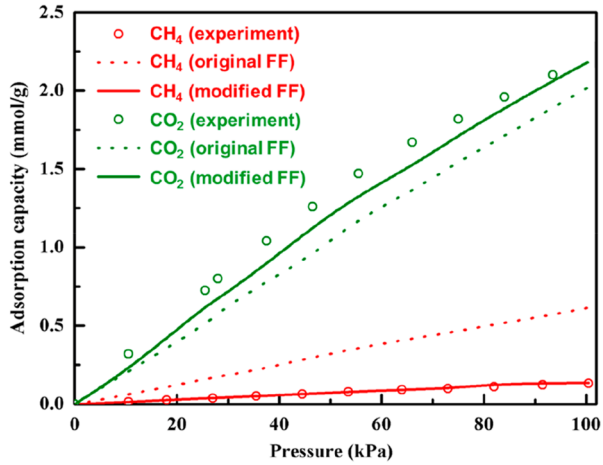

Figure 1. Comparisons between the simulated and experimental results for the adsorption isotherms of pure CH_4 and CO_2 in ZIF-8 at 298 K, respectively.

Table 1. All L-J Parameters Used in This Work

	types	σ (Å)	ε (kcal/mol)
gas molecule	CH_4	3.822	0.27204
	CO_2	3.996	0.37728
ZIF-8	Zn	1.960	0.01250
	N	3.250	0.17000
	C1	3.400	0.08600
	C2	3.400	0.10940
	H1	2.511	0.01500
	H2	2.650	0.01570

DCV-DMC simulation is still computationally expensive although its computational efficiency is higher than the DCV-GCMD simulation. Specifically, the whole computation amount results only from calculating the interaction energies between the gas molecules and the ZIF-8 membrane as well as between the gas molecules themselves since the structure of the ZIF-8 membrane was always rigid during our simulations. Furthermore, the former dominates the whole computation amount. To further speed up the computational efficiency, an appealing option is to calculate the potential energy on the grid, with the so-called Potential Map (PM).[78,79] In other words, the whole permeation region in the simulated system is mapped on a discrete grid, and the interaction energy is not computed at the position of each gas molecule and the ZIF-8 membrane but rather at each grid point. The potential energy calculated at the grid points corresponding to each gas position is then interpolated to obtain the energy on the particles. For convenience, the improved DCV-DMC simulation by us was denoted as the PM-DCV-DMC simulation. This method is much faster than doing a direct computation of the potential energy by summing the contributions of all particles in the system. However, since the resolution of the PM method depends on the size of the grid unit, it would require an extremely fine grid to accurately describe the potential energy. By detailed comparisons, the whole permeation region (i.e., the red dotted region in Figure 2) was divided into $n_x \times n_y \times n_z$ grid points with the distance between two adjacent points no more than 0.24 Å, which is small enough to accurately describe the interaction energy between the gas molecule at any position and the ZIF-8 membrane, as shown in Figure S1 of

https://dx.doi.org/10.1021/acs.jcim.0c00114
J. Chem. Inf. Model. 2020, 60, 2208−2218

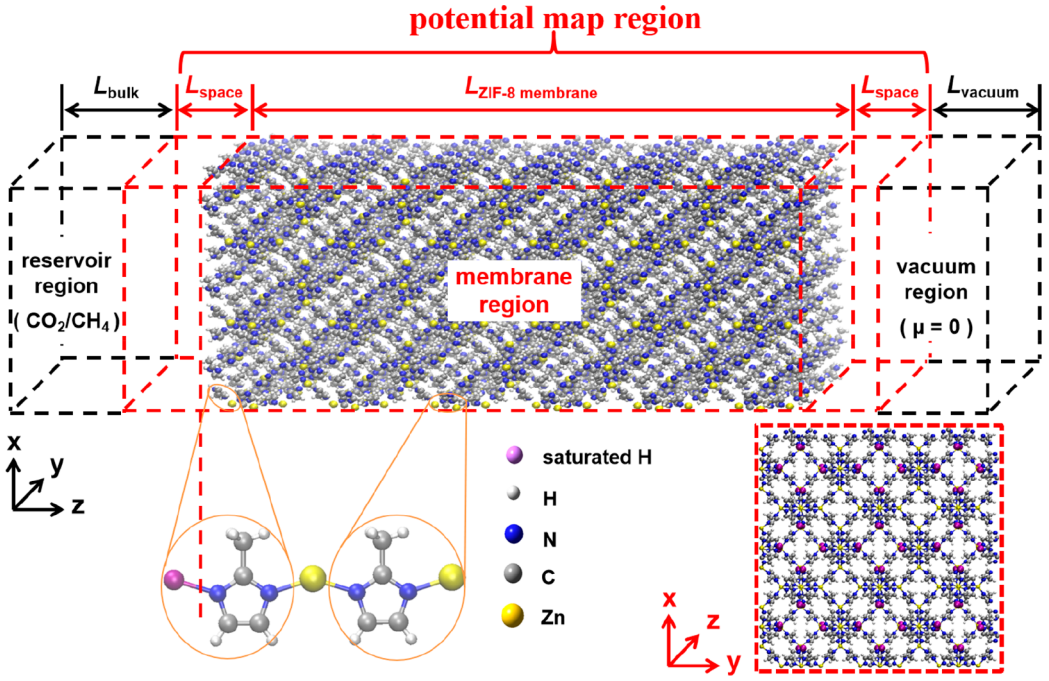

Figure 2. Schematic illustration for the PM-DCV-DMC simulation of the separation behavior of CH_4/CO_2 gas mixtures in the ZIF-8 membrane. All values of $L_{ZIF\text{-}8\ membrane}$, L_{space}, L_{vacuum}, and L_{bulk} at different systems are listed in Table S1 of the Supporting Information.

the Supporting Information. It should be also noted that there is no interaction energy between the gas molecules and the ZIF-8 membrane in two CVs at both ends. Meanwhile, the comparison results in Figure S2 of the Supporting Information clearly demonstrate that each computation time with the DCV-DMC approach is more than that with the DCV-DMC approach by at least 2 orders of magnitude, meaning that the improved PM-DCV-DMC is significantly faster than the conventional DCV-DMC.

As shown in Figure 2, our simulation system consisted of three parts, where the black dotted regions of both the reservoir (i.e., the feed phase) and vacuum parts (i.e., the permeation phase) at both ends represent the control volumes (CVs), while the red dotted region corresponds to the part of membrane permeation. Different chemical potentials were used in two CVs, where the gas molecules in the left-side CV have a high chemical potential, while those in the right-side CV have a low chemical potential. In order to simulate steady-state flux, it is necessary to maintain the densities of each gas component in the reservoir region in equilibrium with the bulk phase, where the density of each component was held constant by the normal GCMC method with the given chemical potential. Therefore, three types of move trials were used in the reservoir region: (1) displacement of a particle, (2) insertion of a particle, and (3) deletion of a particle. Meanwhile, the chemical potential in the vacuum region was always set to zero in this work to produce the density or chemical potential gradient between both the reservoir and vacuum regions. In other words, a particle was removed once it enters into the vacuum region.

On the other hand, the whole permeation region in the middle includes one ZIF-8 membrane and two buffer parts, corresponding to the region covered by PM. The left-side buffer part connects the feed phase with the surface of the ZIF-8 membrane, while the right-side one is between the surface of the ZIF-8 membrane and the vacuum phase. Such buffer parts are favorable to the reproduction of adsorption and desorption behavior of gas molecules on the membrane surfaces, as shown in the previous nonequilibrium simulations of Ozcan and co-workers.[68] In the whole permeation region, only the displacement of particles is permitted by using the grand canonical MC method and is expected to distribute according to the chemical potential gradient between both the reservoir and vacuum regions.

In our PM-DCV-DMC simulation, the type of molecule in the mixture was chosen with equal probability at each move. Meanwhile, displacement, insertion, and deletion moves were done with a ratio of 48:1:1 for the whole simulation system since the number of particles with the displacement is much larger than those with the insertion or deletion move. It should be noted that this ratio is large enough to guarantee at least one gas molecule permeating the vacuum region per 2×10^6 steps to obtain reliable statistical results. It should be noted that the maximum displacement, d_{max}, is a key parameter, which controls the convergence of the Markov chain and determines the reliability of simulation results. A large d_{max} value can accelerate the system to reach equilibrium, but it may not be able to reflect the realistic molecular distribution inside the ZIF-8 membrane once it is beyond a certain value. Therefore, it is necessary to optimize the d_{max} to balance both the simulation efficiency and stability. The main determinant of the d_{max} parameter is the density of the system.[72,75−77] Therefore, based on the previous DCV-DMC simulations for the membrane transport,[72−77] the d_{max} value in the range from 2 to 5 Å was selected for testing. We compared different density distributions along the z direction for the gas mixture with different d_{max} values. As shown in Figure S3 of the Supporting Information, the d_{max} value of 3 Å is optimum since the concentration gradient inside the ZIF-8 membrane is almost linearly proportional, which is consistent with the conclusion reported by Ozcan et al.[68] Then, the PM-DCV-DMC simulation for each simulation system was run for over 3

https://dx.doi.org/10.1021/acs.jcim.0c00114
J. Chem. Inf. Model. 2020, 60, 2208−2218

$\times 10^{10}$ steps with the first 1×10^{10} steps for equilibration, and the configurations were recorded every 1×10^{4} steps after equilibration.

3. RESULTS AND DISCUSSION

3.1. Effect of Composition on Membrane Separation.

First, we explore the effect of feed composition on the separation properties of the CH_4/CO_2 mixtures in the ZIF-8 membrane. The calculated density distributions along the z direction for the gas mixtures with different feed compositions are depicted in Figure 3. It is clear from this figure that, along the permeation direction, all density profiles for both CO_2 and CH_4 first show a sharp increase in the individual maximum within the first outermost unit cell at the feed side. After that, the density profiles start to present a gradually decaying trend until the particles are removed beyond the osmotic side. This indicates that the CO_2 and CH_4 molecules are initially adsorbed on the outside membrane surface due to the strong adsorption affinity of ZIF-8 for the CH_4/CO_2 mixtures, and then they will diffuse into the membrane and aggregate together in the region close to the feed side. Upon further adsorption of gas molecules, the initially aggregated molecules will gradually propagate toward the permeation side. Additionally, as the ZIF-8 membrane is a crystal material with periodic cages and pores, the density profiles exhibit the periodic fluctuated distribution (see Figure 3). Meanwhile, it can be noted that the density of CO_2 is much higher than that of CH_4 in all mixture compositions, which can be explained by the much stronger adsorption capacity of the ZIF-8 membrane for CO_2 over CH_4.[19,21,81] Accordingly, the relative flux of CO_2 is found to be always much larger than that of CH_4 although the former displays a monotonous decrease while the latter shows an obvious increase as the mole fraction of CH_4 increases, as shown in Figure S4 of the Supporting Information.

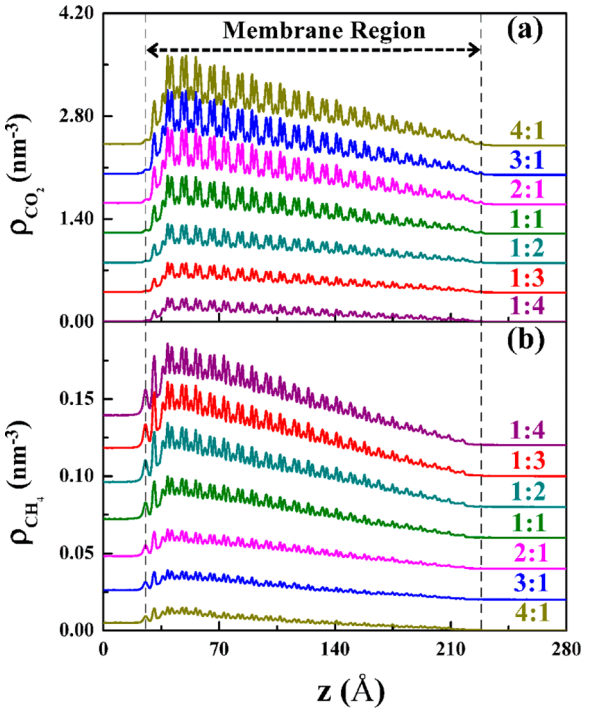

Figure 3. Density profiles along the z direction for (a) CO_2 and (b) CH_4 in the mixtures with different feed compositions at 300 K and 1 atm. The two vertical dashed lines indicate the boundaries of the membrane region. To enhance visual clarity, the CO_2 profiles for the compositions of 1/4, 1/3, 1/2, 1/1, 2/1, 3/1, and 4/1 are shifted upward by 0, 0.4, 0.8, 1.2, 1.6, 2.0, and 2.4 nm^{-3}, respectively, and the CH_4 profiles for the compositions of 4/1, 3/1, 2/1, 1/1, 1/2, 1/3, and 1/4 are separately shifted upward by 0, 0.02, 0.04, 0.06, 0.08, 0.1, and 0.12 nm^{-3}.

Next, the corresponding selectivity profiles of $\alpha_{CO_2/CH_4}(z)$ along the permeation direction for the CH_4/CO_2 mixtures in the ZIF-8 membrane were evaluated (see Figure 4). The selectivity profile of $\alpha_{CO_2/CH_4}(z)$ can be defined as

$$\alpha_{CO_2/CH_4}(z) = \frac{\rho_{CO_2}(z)/\rho_{CH_4}(z)}{\rho_{CO_2,bulk}/\rho_{CH_4,bulk}} \quad (1)$$

where $\rho_i(z)$ is the local density of component i within a layer at position z, and $\rho_{i,bulk}$ is the bulk density of component i. Figure 4 shows that there is negligible change among all the selectivity profiles. Specifically, the selectivity profiles of $\alpha_{CO_2/CH_4}(z)$ first increase gradually but with trivial fluctuations along the permeation direction. After that, the selectivity goes up rapidly to the maximum and follows a sharp decrease near the membrane surface at the permeation side. The first increase can be explained by the higher accumulated CO_2 molecules which resulted from the stronger affinity of ZIF-8 for CO_2. As the CO_2 molecules approach the permeation side, the affinity interactions from the ZIF-8 become the dominant factor that prevents the CO_2 desorption. This makes the selectivity increase sharply, but it also leads to the final separation selectivity lower than the intramembrane selectivity. Such results indicate that the parts near membrane surfaces at both ends play a key role in determining the separation selectivity. Hereto, one can conclude that the permeation of the ZIF-8 membrane is mainly due to adsorption control, and gas composition changes are almost completely independent of selectivity.

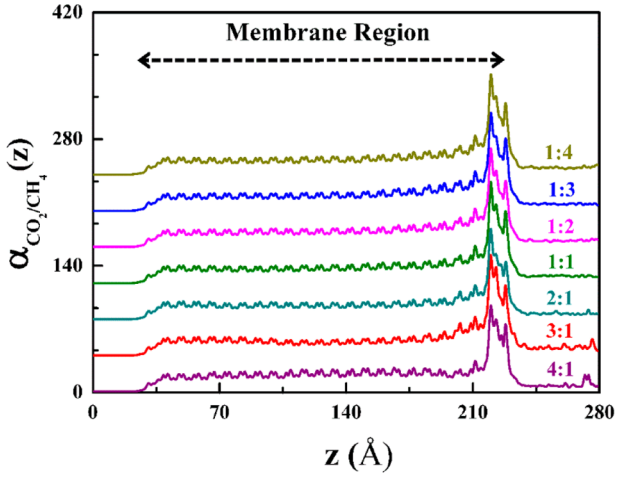

Figure 4. Selectivity profiles of $\alpha_{CO_2/CH_4}(z)$ along the permeation direction for the CH_4/CO_2 mixtures with different feed compositions in the ZIF-8 membrane. Note: the two vertical dashed lines indicate the boundaries of the membrane region. To enhance visual clarity, the selectivity profiles for the compositions of 1/4, 1/3, 1/2, 1/1, 2/1, 3/1, and 4/1 are shifted upward by 0, 40, 80, 120, 160, 200, and 240, respectively.

https://dx.doi.org/10.1021/acs.jcim.0c00114
J. Chem. Inf. Model. 2020, 60, 2208−2218

3.2. Effect of Temperature on Membrane Separation.

It is well-accepted that the temperature remarkedly influences the motion of gas molecules. In this context, we also explored the temperature effect on the separation performance of the ZIF-8 membrane for equimolar CH_4/CO_2 mixtures at ambient pressure. First, the density profiles of gas molecules inside the membrane under different simulation temperatures were calculated, as listed in Figure 5, and here the investigated

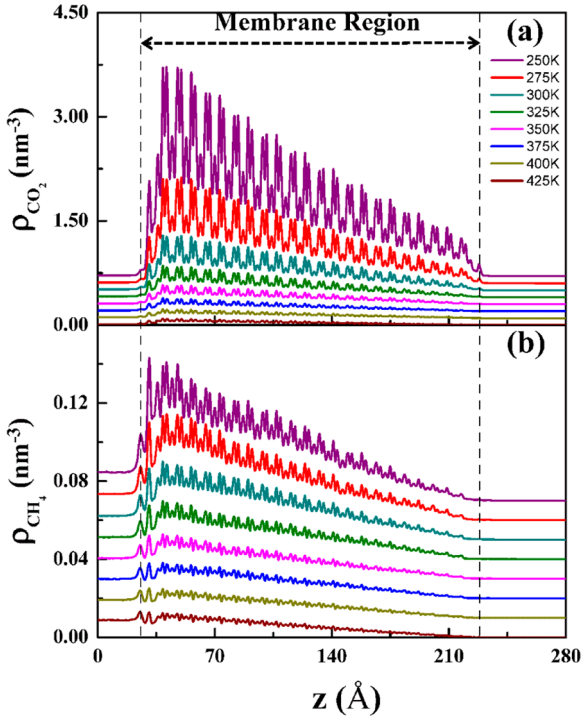

Figure 5. Density profiles along the z direction for (a) CO_2 and (b) CH_4 in the equimolar mixtures at different temperatures. The two vertical dashed lines indicate the boundaries of the membrane region. To enhance visual clarity, the CO_2 (CH_4) density profiles for the temperatures of 250, 275, 300, 325, 350, 375, 400, and 425 K are shifted upward by 0 (0), 0.1 (0.01), 0.2 (0.02), 0.3 (0.03), 0.4 (0.04), 0.5 (0.05), 0.6 (0.06), and 0.7 (0.07) nm^{-3}, respectively.

temperature varies from 250 to 425 K with an increment of 25 K. Figure 5 demonstrates that all the density profiles initially go up rapidly and then follow a declined trend with a periodic fluctuation, which is in analogy with the distribution in Figure 3. However, one thing is worth noting that, with the increase of the temperature, there is a significant decrease for the densities of both CO_2 and CH_4, and the fluctuation amplitude of the densities also becomes smaller with respect to the higher temperature. This is consistent with the fact that low temperature favors the physical adsorption of gas molecules inside the porous materials, which primarily ascribes to the fact that the decreased temperature will lower the diffusion rate of both CO_2 and CH_4 and in turn it would boost the aggregation of gas molecules inside the porous cages of membrane. Besides, for each temperature, the density of CO_2 is much larger than that of CH_4, particularly at the lower temperature. This uncovers that a lower temperature would be favorable for the preferred adsorption of CO_2 inside the ZIF-8 membrane, and thereby it would benefit the separation of CO_2 from CH_4 in the mixtures. Meanwhile, another thing that should be mentioned is that the density distribution remains almost unchanged when the temperature is higher than 400 K, demonstrating that the diffusion of gas molecules becomes barrierless since the kinetic energies of gas molecules exceed their diffusion energy barrier at this temperature.

Accordingly, we calculated the selectivity profiles of $\alpha_{CO_2/CH_4}(z)$ along the permeation direction for the equimolar CH_4/CO_2 mixture in the ZIF-8 membrane at different temperatures, as depicted in Figure 6. The variation trend

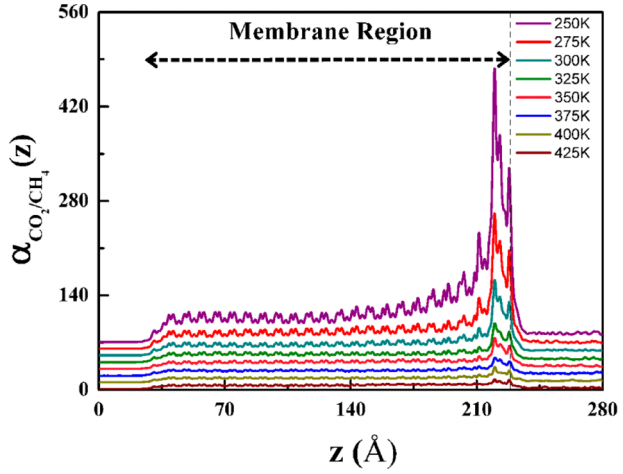

Figure 6. Selectivity profiles of $\alpha_{CO_2/CH_4}(z)$ along the permeation direction for the equimolar CH_4/CO_2 mixture in the ZIF-8 membrane at different temperatures. Note: the two vertical dashed lines indicate the boundaries of the membrane region. To enhance visual clarity, the selectivity profiles for the temperatures of 250, 275, 300, 325, 350, 375, 400, and 425 K are shifted upward by 0, 10, 20, 30, 40, 50, 60, and 70, respectively.

exhibited in the figure is similar to that observed in Figure 4, but there is a big difference in the region close to the permeation side, where the selectivity values sharply rise upon the decrease of temperature from 400 to 250 K (see Figure 6). This mainly originates from that fact that the lower temperature would hinder the CO_2 molecules to diffuse toward the permeation side of the membrane owing to the stronger adsorption affinity imposed by the ZIF-8 framework for CO_2 molecules. As a result, it would lead to a higher accumulation of CO_2 molecules inside the membrane compared to the CH_4 molecules, thus contributing to a higher selectivity and fluctuation amplitude for CO_2 molecules. Aside from that, when the temperature increases from 400 and 425 K, those selectivity profiles almost remain the same, in agreement with the density distribution results in Figure 5. To this end, it can be concluded that the temperature plays a key role in the separation performance of the ZIF-8 membrane, and a relatively low temperature would be a great strategy to separate the CH_4/CO_2 mixtures.

3.3. Effect of Pressure on Membrane Separation.

Figure 7 illustrates the dependence on the external pressure of the density distributions for the gas molecules in equimolar CH_4/CO_2 mixtures at 300 K. The distribution profiles for CO_2 molecules in Figure 7a display a similar variation trend as those in Figures 3a and 5a, but the density values show some unique correlations with the external pressure. When the pressure changes from 1 to 10 atm, there is an obvious increase in the density of CO_2; however, the corresponding values then remain scarcely changed with the enhancement of pressure

https://dx.doi.org/10.1021/acs.jcim.0c00114
J. Chem. Inf. Model. 2020, 60, 2208−2218

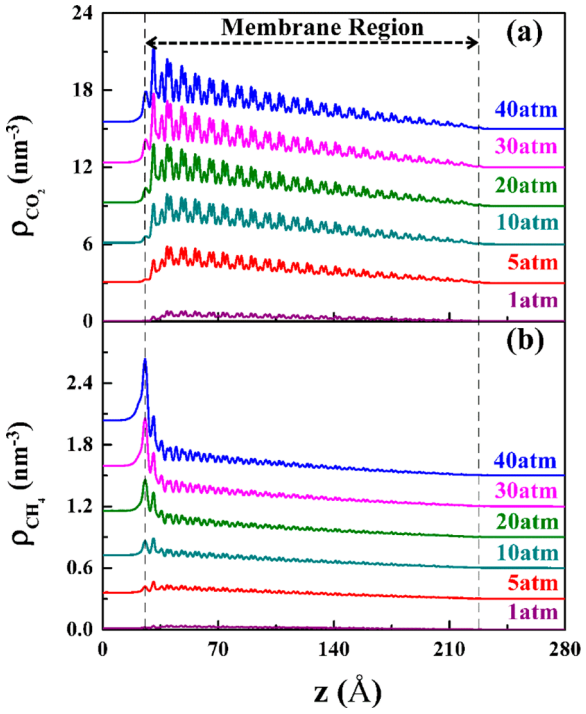

Figure 7. Density profiles along the z direction for (a) CO_2 and (b) CH_4 in the equimolar mixtures at different pressures. The two vertical dashed lines indicate the boundaries of membrane region. To enhance visual clarity, the CO_2 (CH_4) density profiles for the pressures of 1.0, 5.0, 10.0, 20.0, 30.0, and 40.0 atm are shifted upward by 0.0 (0.0), 3.0 (0.35), 6.0 (0.7), 9.0 (1.05), 12.0 (1.4), and 15.0 (1.75) nm^{-3}, respectively.

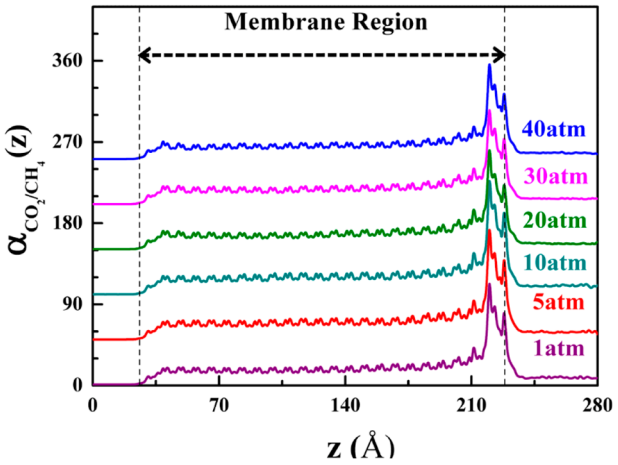

Figure 8. Selectivity profiles of $\alpha_{CO_2/CH_4}(z)$ along the permeation direction for the equimolar CH_4/CO_2 mixture in the ZIF-8 membrane at different pressures. Note: the temperature is 300 K, and the two vertical dashed lines indicate the boundaries of the membrane region. To enhance visual clarity, the selectivity profiles for the pressures of 1.0, 5.0, 10.0, 20.0, 30.0, and 40.0 atm are shifted upward by 0, 50, 100, 150, 200, and 250, respectively.

from 10 to 40 atm. This is because increasing pressure can lead to an obvious increase in the number of particles adsorbed in the ZIF membrane at low pressures. Once the adsorption sites of the internal membrane surface area are saturated by the gas molecules, further increasing the pressure cannot give rise to a significant increase for the density anymore. On the other hand, for the distributions of the CH_4 molecule in Figure 7b, it clearly shows that the densities reach the maximum values at the boundary of the membrane region and then sharply decrease within several fluctuations, which is obviously different from those in Figures 3b and 5b, especially under the high pressures. This primarily derives from the fact that the exerted high pressure in the feed region would preferentially prompt the CO_2 molecules to diffuse into the ZIF-8 membrane due to the existence of specific adsorption sites for CO_2 inside the porous cages. In this case, the CH_4 molecules would first reside and accumulate on the external surface of the ZIF-8 membrane, resulting in a maximum density at the boundary of the feed region of membrane, as displayed in Figure 7b.

Figure 8 represents the selectivity profiles along the permeation direction for the equimolar CH_4/CO_2 mixture at different pressures. It is obvious from this figure that, for each pressure, the variation trend of the selectivity along the permeation direction is in good agreement with that displayed in Figures 4 and 6. With the augment of pressure, it is certain that the concentration of both CO_2 and CH_4 molecules inside the ZIF-8 membrane will increase as shown in Figure 7. Nevertheless, compared to the CH_4 molecules, the CO_2 molecules have stronger interactions with the ZIF-8 framework. Therefore, it would be much more beneficial for the accumulation of CO_2 molecules inside the membrane close to the feed side, which is conducive to a slight increase for the selectivity of the CH_4/CO_2 mixture. However, it should be pointed out that all the selectivity profiles do not show a sensitive response to the applied external pressure, peculiarly the high pressure. This is mainly because the internal surface area of the ZIF-8 membrane has limited adsorption sites for the gas molecules, and the selectivity of the CH_4/CO_2 mixture would reach the maximum value once those sites are fully occupied by the gas molecules. As shown in Figure S5 of the Supporting Information, we can find that CO_2 molecules in ZIF-8 almost reach the adsorption saturation when the pressure increases up to 30 atm. Then further increasing the pressure would enable a large amount of gas molecules to accumulate on the external surfaces of the ZIF-8 membrane and block the pores entrance, and in turn the selectivity of the CH_4/CO_2 mixture would not increase, even showing a slight decrease.

3.4. Overall Selectivity. To quantitatively characterize the separation performance of the ZIF-8 membrane, the overall separation selectivity (α_{CO_2/CH_4}) of the ZIF-8 membrane for the binary CH_4/CO_2 mixture was estimated with the following definition

$$\alpha_{CO_2/CH_4} = \frac{x_{CO_2}/x_{CH_4}}{y_{CO_2}/y_{CH_4}} \quad (2)$$

where x_i is the accumulated mole fraction of component i into the vacuum region, and y_i is the corresponding mole fraction in the reservoir region. First, the results in Figure 9a show that the overall selectivity of the ZIF-8 membrane for the CH_4/CO_2 mixture slightly changes in the range of 7.75 and 8.5 among all studied feed compositions. Such composition-dependent selectivity variation is consistent with the result calculated by McEwen et al.[82] using the IAST from the experimental isotherms for pure gases. More importantly, our calculated selectivities of α_{CO_2/CH_4} are very close to the experimental result of around 7 reported by Venna et al.[21] for the CH_4/CO_2 gas mixtures in the ZIF-8 membrane. Figures

https://dx.doi.org/10.1021/acs.jcim.0c00114
J. Chem. Inf. Model. 2020, 60, 2208−2218

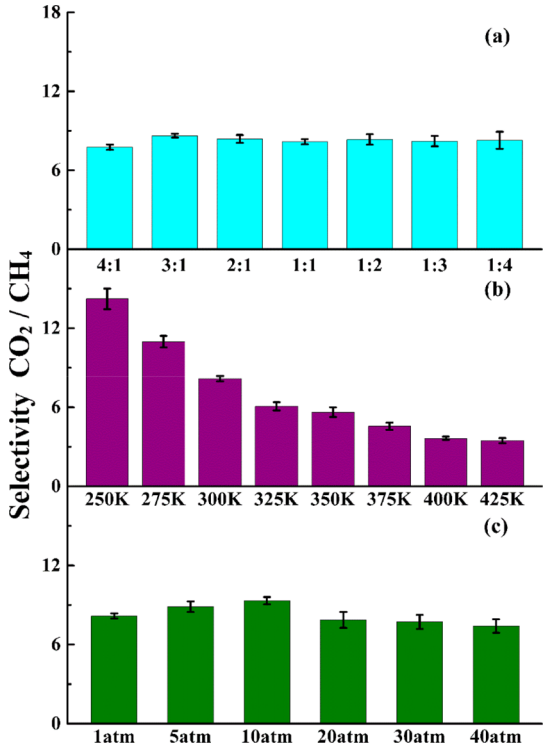

Figure 9. Separation selectivity of the ZIF-8 membrane for the CH_4/CO_2 mixture with different (a) feed compositions, (b) temperatures, and (c) pressures. Note: the feed composition in (b) and (c) is 1:1; the pressure and temperature in (a) correspond to 1 atm and 300 K; the pressure in (b) is 1 atm; and the temperature in (c) is 300 K.

9b and 9c illustrate the effect of temperature and pressure on the selectivity of the ZIF-8 membrane for equimolar CH_4/CO_2 mixtures, respectively. It can be observed from Figure 9b that the selectivity exponentially decreases from 14.23 to 3.47 with the temperature increasing from 250 to 425 K, suggesting that a lower temperature would improve the separation performance of the ZIF-8 membrane, in good accordance with the experimental results reported by Bux and coauthors.[19] Additionally, the results in Figure 9c exhibit that the overall selectivity has a slight enhancement from 8.17 to 9.33 with the pressure varying from 1 to 10 atm. Afterward, the selectivity value falls to a constant value of 7.75 upon further increasing the pressure from 20 to 40 atm. Finally, we can conclude that the separation selectivity of the ZIF-8 membrane for the CH_4/CO_2 mixture is in close relation to the temperature but slightly dependent on the feed composition and pressure, indicative of the fact that the permeation process of the ZIF-8 membrane is remarkedly determined and controlled by the diffusion rates of gas molecules inside the nanoporous membrane.

4. CONCLUSIONS

In this work, a series of nonequilibrium PM-DCV-DMC simulations developed by us have been carried out to explore the separation selectivity of CH_4/CO_2 gas mixtures in the ZIF-8 membrane with a thickness of up to about 20 nm, where the corresponding potential maps are introduced into the conventional DCV-DMC method to further speed up the computational efficiency. Our simulation results clearly show that all densities along the permeation direction of both CH_4 and CO_2 molecules initially show a sharp increase in the individual maximum within the first outermost unit cell at the feed side and follow a long fluctuating decrease process. Accordingly, the corresponding selectivity profiles of $\alpha_{CO_2/CH_4}(z)$ along the permeation direction are found to initially display a long fluctuating increase to the individual maximum and follow a sharp decrease near the membrane surface at the permeation side. Such density and selectivity profiles along the permeation direction indicate that the parts near membrane surfaces at both ends play a key role in determining the separation selectivity of CH_4/CO_2 gas mixtures in the ZIF-8 membrane. Furthermore, the effects of feed composition, temperature, and pressure on the relevant separation selectivity are also discussed in detail, where the temperature has a greater influence on the separation selectivity than the feed composition and pressure. More importantly, the predicted separation selectivities from our PM-DCV-DMC simulations are well consistent with the previously experimental results. Therefore, our nonequilibrium simulation results in this work provide a complete molecular-level picture of the density and selectivity profiles of gas molecules in the ZIF-8 membrane with the actual thickness, which is of great importance for experimental scientists to understand the separation behavior of gas mixtures in ZIF membranes.

■ ASSOCIATED CONTENT

Supporting Information

The Supporting Information is available free of charge at https://pubs.acs.org/doi/10.1021/acs.jcim.0c00114.

Details of simulation systems; comparisons in both density profiles and computation times between DCV-DMC and PM-DCV-DMC methods; density profiles with different maximum displacement values; simulated fluxes of gas molecules in ZIF-8 membrane; and simulated adsorption isotherms of gas molecules in ZIF-8 (PDF)

■ AUTHOR INFORMATION

Corresponding Authors

Xiangshu Chen − *Institute of Advanced Materials (IAM), State-Province Joint Engineering Laboratory of Zeolite Membrane Materials, College of Chemistry and Chemical Engineering, Jiangxi Normal University, Nanchang 330022, People's Republic of China;* orcid.org/0000-0003-2378-2271; Email: cxs66cn@jxnu.edu.cn

Zhen Yang − *Institute of Advanced Materials (IAM), State-Province Joint Engineering Laboratory of Zeolite Membrane Materials, College of Chemistry and Chemical Engineering, Jiangxi Normal University, Nanchang 330022, People's Republic of China;* orcid.org/0000-0002-5205-3281; Email: yangzhen@jxnu.edu.cn

Authors

Zheng Wan − *Institute of Advanced Materials (IAM), State-Province Joint Engineering Laboratory of Zeolite Membrane Materials, College of Chemistry and Chemical Engineering, Jiangxi Normal University, Nanchang 330022, People's Republic of China*

Guobing Zhou − *Institute of Advanced Materials (IAM), State-Province Joint Engineering Laboratory of Zeolite Membrane Materials, College of Chemistry and Chemical Engineering, Jiangxi Normal University, Nanchang 330022, People's Republic of China; School of Chemical, Biological and Materials*

Engineering, University of Oklahoma, Norman, Oklahoma 73019, United States

Zhongyang Dai − *Shenzhen Institute of Advanced Technology, Chinese Academy of Sciences, Shenzhen 518055, People's Republic of China; National Supercomputing Center in Shenzhen, Shenzhen 518055, People's Republic of China*

Li Li − *Institute of Advanced Materials (IAM), State-Province Joint Engineering Laboratory of Zeolite Membrane Materials, College of Chemistry and Chemical Engineering, Jiangxi Normal University, Nanchang 330022, People's Republic of China*

Na Hu − *Institute of Advanced Materials (IAM), State-Province Joint Engineering Laboratory of Zeolite Membrane Materials, College of Chemistry and Chemical Engineering, Jiangxi Normal University, Nanchang 330022, People's Republic of China*

Complete contact information is available at: https://pubs.acs.org/10.1021/acs.jcim.0c00114

Author Contributions

[⊥]Z.W. and G.Z. contributed equally to this work and should be considered as first coauthors.

Notes

The authors declare no competing financial interest.

■ ACKNOWLEDGMENTS

This work was supported by the National Natural Science Foundation of China (Nos. 21306070, 21863005, and 21868013), the Natural Science Foundation of Jiangxi Province (No. 20171BAB203012), the Special Program for Applied Research on Super Computation of the NSFC-Guangdong Joint Fund (the second phase) under Grant No. U1501501, and the Sponsored Program for Cultivating Youths of Outstanding Ability in Jiangxi Normal University.

■ REFERENCES

(1) Han, S. S.; Mendoza-Cortés, J. L.; Goddard, W. A., III Recent Advances on Simulation and Theory of Hydrogen Storage in Metal-Organic Frameworks and Covalent Organic Frameworks. *Chem. Soc. Rev.* **2009**, *38*, 1460−1476.

(2) Li, J. R.; Sculley, J.; Zhou, H. C. Metal-Organic Frameworks for Separations. *Chem. Rev.* **2012**, *112*, 869−932.

(3) Shah, M.; McCarthy, M. C.; Sachdeva, S.; Lee, A. K.; Jeong, H. K. Current Status of Metal Organic Framework Membranes for Gas Separations: Promises and Challenges. *Ind. Eng. Chem. Res.* **2012**, *51*, 2179−2199.

(4) Denny, M. S.; Moreton, J. C.; Benz, L.; Cohen, S. M. Metal-Organic Frameworks for Membrane-based Separations. *Nat. Rev. Mater.* **2016**, *1*, 16078−16095.

(5) Chen, B. L.; Yang, Z. X.; Zhu, Y. Q.; Xia, Y. D. Zeolitic Imidazolate Framework Materials: Recent Progress in Synthesis and Applications. *J. Mater. Chem. A* **2014**, *2*, 16811−16831.

(6) Kaneti, Y. V.; Dutta, S.; Hossain, M. S. A.; Shiddiky, M. J. A.; Tung, K. L.; Shieh, F. K.; Tsung, C. K.; Wu, K. C.; Yamauchi, Y. Strategies for Improving the Functionality of Zeolitic Imidazolate Frameworks: Tailoring Nanoarchitectures for Functional Applications. *Adv. Mater.* **2017**, *29*, 1700213.

(7) Bhattacharjee, S.; Jang, M. S.; Kwon, H. J.; Ahn, W. S. Zeolitic Imidazolate Frameworks: Synthesis, Functionalization, and Catalytic/Adsorption Applications. *Catal. Surv. Asia* **2014**, *18*, 101−127.

(8) Park, K. S.; Ni, Z.; Cote, A. P.; Choi, J. Y.; Huang, R. D.; Uribe-Romo, F. J.; Chae, H. K.; O'Keeffe, M.; Yaghi, O. M. Exceptional Chemical and Thermal Stability of Zeolitic Imidazolate Frameworks. *Proc. Natl. Acad. Sci. U. S. A.* **2006**, *103*, 10186−10191.

(9) Wang, B.; Cote, A. P.; Furukawa, H.; O'Keeffe, M.; Yaghi, O. M. Colossal Cages in Zeolitic Imidazolate Frameworks as Selective Carbon Dioxide Reservoirs. *Nature* **2008**, *453*, 207−211.

(10) Banerjee, R.; Phan, A.; Wang, B.; Knobler, C.; Furukawa, H.; O'Keeffe, M.; Yaghi, O. M. High-throughput Synthesis of Zeolitic Imidazolate Frameworks and Application to CO_2 Capture. *Science* **2008**, *319*, 939−943.

(11) Phan, A.; Doonan, C. J.; Uribe-Romo, F. J.; Knobler, C. B.; O'Keeffe, M.; Yaghi, O. M. Synthesis, Structure, and Carbon Dioxide Capture Properties of Zeolitic Imidazolate Frameworks. *Acc. Chem. Res.* **2010**, *43*, 58−67.

(12) Pimentel, B. R.; Parulkar, A.; Zhou, E. K.; Brunelli, N. A.; Lively, R. P. Zeolitic Imidazolate Frameworks: Next-generation Materials for Energy-efficient Gas Separations. *ChemSusChem* **2014**, *7*, 3202−3240.

(13) Yao, J. F.; Wang, H. T. Zeolitic Imidazolate Framework Composite Membranes and Thin Films: Synthesis and Applications. *Chem. Soc. Rev.* **2014**, *43*, 4470−4493.

(14) Thornton, A. W.; Dubbeldam, D.; Liu, M. S.; Ladewig, B. P.; Hill, A. J.; Hill, M. R. Feasibility of Zeolitic Imidazolate Framework Membranes for Clean Energy Applications. *Energy Environ. Sci.* **2012**, *5*, 7637−7646.

(15) Bux, H.; Liang, F. Y.; Li, Y. S.; Cravillon, J.; Wiebcke, M.; Caro, J. Zeolitic Imidazolate Framework Membrane with Molecular Sieving Properties by Microwave-assisted Solvothermal Synthesis. *J. Am. Chem. Soc.* **2009**, *131*, 16000−16001.

(16) Li, Y. S.; Liang, F. Y.; Bux, H.; Yang, W. S.; Caro, J. Zeolitic Imidazolate Framework ZIF-7 based Molecular Sieve Membrane for Hydrogen Separation. *J. Membr. Sci.* **2010**, *354*, 48−54.

(17) Li, Y. S.; Bux, H.; Feldhoff, A.; Li, G. L.; Yang, W. S.; Caro, J. Controllable Synthesis of Metal-Organic Frameworks: From MOF Nanorods to Oriented MOF Membranes. *Adv. Mater.* **2010**, *22*, 3322−3326.

(18) Li, Y. S.; Liang, F. Y.; Bux, H.; Feldhoff, A.; Yang, W. S.; Caro, J. Molecular Sieve Membrane: Supported Metal-Organic Framework with High Hydrogen Selectivity. *Angew. Chem., Int. Ed.* **2010**, *49*, 548−551.

(19) Bux, H.; Chmelik, C.; van Baten, J. M.; Krishna, R.; Caro, J. Novel MOF-Membrane for Molecular Sieving Predicted by IR-Diffusion Studies and Molecular Modeling. *Adv. Mater.* **2010**, *22*, 4741−4743.

(20) Yeo, Z. Y.; Zhu, P. W.; Mohamed, A. R.; Chai, S. P. A Well Inter-grown ZIF-8 Membrane Synthesized via Two-step Hydrothermal Synthesis on Coarse α-Al_2O_3 Support. *Mater. Lett.* **2014**, *129*, 162−165.

(21) Venna, S. R.; Carreon, M. A. Highly Permeable Zeolite Imidazolate Framework-8 Membranes for CO_2/CH_4 Separation. *J. Am. Chem. Soc.* **2010**, *132*, 76−78.

(22) Gong, X.; Wang, Y. J.; Kuang, T. R. ZIF-8-based Membranes for Carbon Dioxide Capture and Separation. *ACS Sustainable Chem. Eng.* **2017**, *5*, 11204−11214.

(23) Shekhah, O.; Swaidan, R.; Belmabkhout, Y.; Plessis, M.; Jacobs, T.; Barbour, L. J.; Pinnau, I.; Eddaoudi, M. The Liquid Phase Epitaxy Approach for the Successful Construction of Ultra-thin and Defect-free ZIF-8 Membranes: Pure and Mixed Gas Transport Study. *Chem. Commun.* **2014**, *50*, 2089−2092.

(24) Bux, H.; Feldhoff, A.; Cravillon, J.; Wiebcke, M.; Li, Y. S.; Caro, J. Oriented Zeolitic Imidazolate Framework-8 Membrane with Sharp H_2/C_3H_8 Molecular Sieve Separation. *Chem. Mater.* **2011**, *23*, 2262−2269.

(25) Pan, Y. C.; Lai, Z. P. Sharp Separation of C2/C3 Hydrocarbon Mixtures by Zeolitic Imidazolate Framework-8 (ZIF-8) Membranes Synthesized in Aqueous Solutions. *Chem. Commun.* **2011**, *47*, 10275−10277.

(26) Pan, Y. C.; Li, T.; Lestari, G.; Lai, Z. P. Effective Separation of Propylene/Propane Binary Mixtures by ZIF-8 Membranes. *J. Membr. Sci.* **2012**, *390*, 93−98.

(27) Hara, N.; Yoshimune, M.; Negishi, H.; Haraya, K.; Hara, S.; Yamaguchi, T. Diffusive Separation of Propylene/Propane with ZIF-8 Membranes. *J. Membr. Sci.* **2014**, *450*, 215−223.

(28) Jomekian, A.; Behbahani, R. M.; Mohammadi, T.; Kargari, A. CO_2/CH_4 Separation by High Performance Co-Casted ZIF-8/Pebax

1657/PES Mixed Matrix Membrane. *J. Nat. Gas Sci. Eng.* **2016**, *31*, 562−574.
(29) Zeeshan, M.; Keskin, S.; Uzun, A. Enhancing CO_2/CH_4 and CO_2/N_2 Separation Performances of ZIF-8 by Post-Synthesis Modification with [BMIM][SCN]. *Polyhedron* **2018**, *155*, 485−492.
(30) Hou, Q. Q.; Wu, Y.; Zhou, S.; Wei, Y. Y.; Caro, J.; Wang, H. H. Ultra-Tuning of the Aperture Size in Stiffened ZIF-8_Cm Frameworks with Mixed-Linker Strategy for Enhanced CO_2/CH_4 Separation. *Angew. Chem., Int. Ed.* **2019**, *58*, 327−331.
(31) Huang, Y. Y.; Liu, D. H.; Liu, Z. P.; Zhong, C. L. Synthesis of Zeolitic Imidazolate Framework Membrane using Temperature-switching Synthesis Strategy for Gas Separation. *Ind. Eng. Chem. Res.* **2016**, *55*, 7164−7170.
(32) Forman, E. M.; Pimentel, B. R.; Ziegler, K. J.; Lively, R. P.; Vasenkov, S. Microscopic Diffusion of Pure and Mixed Methane and Carbon Dioxide in ZIF-11 by High Field Diffusion NMR. *Microporous Mesoporous Mater.* **2017**, *248*, 158−163.
(33) Huang, A. S.; Bux, H.; Steinbach, F.; Caro, J. Molecular-Sieve Membrane with Hydrogen Permselectivity: ZIF-22 in LTA Topology Prepared with 3-Aminopropyltriethoxysilane as Covalent linker. *Angew. Chem., Int. Ed.* **2010**, *49*, 4958−4961.
(34) Liu, Y. Y.; Hu, E. P.; Khan, E. A.; Lai, Z. P. Synthesis and Characterization of ZIF-69 Membranes and Separation for CO_2/CO Mixture. *J. Membr. Sci.* **2010**, *353*, 36−40.
(35) Liu, Y. Y.; Zeng, G. F.; Pan, Y. C.; Lai, Z. P. Synthesis of Highly c-oriented ZIF-69 Membranes by Secondary Growth and Their Gas Permeation Properties. *J. Membr. Sci.* **2011**, *379*, 46−51.
(36) Gücüyener, C.; van den Bergh, J.; Gascon, J.; Kapteijn, F. Ethane/Ethene Separation Turned on Its Head: Selective Ethane Adsorption on the Metal-Organic Framework ZIF-7 through a Gate-Opening Mechanism. *J. Am. Chem. Soc.* **2010**, *132*, 17704−17706.
(37) van den Bergh, J.; Gücüyener, C.; Pidko, E. A.; Hensen, E. J. M.; Gascon, J.; Kapteijn, F. Understanding the Anomalous Alkane Selectivity of ZIF-7 in the Separation of Light Alkane/Alkene Mixtures. *Chem. - Eur. J.* **2011**, *17*, 8832−8840.
(38) Dong, X. L.; Huang, K.; Liu, S. N.; Ren, R. F.; Jin, W. Q.; Lin, Y. S. Synthesis of Zeolitic Imidazolate Framework-78 Molecular-Sieve Membrane: Defect Formation and Elimination. *J. Mater. Chem.* **2012**, *22*, 19222−19227.
(39) Huang, A. S.; Dou, W.; Caro, J. Steam-stable Zeolitic Imidazolate Framework ZIF-90 Membrane with Hydrogen Selectivity through Covalent Functionalization. *J. Am. Chem. Soc.* **2010**, *132*, 15562−15564.
(40) Huang, A. S.; Caro, J. Covalent Post-Functionalization of Zeolitic Imidazolate Framework ZIF-90 Membrane for Enhanced Hydrogen Selectivity. *Angew. Chem., Int. Ed.* **2011**, *50*, 4979−4982.
(41) Huang, A. S.; Wang, N. Y.; Kong, C. L.; Caro, J. Organosilica-Functionalized Zeolitic Imidazolate Framework ZIF-90 Membrane with High Gas-separation Performance. *Angew. Chem., Int. Ed.* **2012**, *51*, 10551−10555.
(42) Cacho-Bailo, F.; Caro, G.; Etxeberría-Benavides, M.; Karvan, Q.; Téllez, C.; Coronas, J. High Selectivity ZIF-93 Hollow Fiber Membranes for Gas Separation. *Chem. Commun.* **2015**, *51*, 11283−11285.
(43) Huang, A. S.; Chen, Y. F.; Wang, N. Y.; Hu, Z. Q.; Jiang, J. W.; Caro, J. A Highly Permeable and Selective Zeolitic Imidazolate Framework ZIF-95 Membrane for H_2/CO_2 Separation. *Chem. Commun.* **2012**, *48*, 10981−10983.
(44) Wang, N. Y.; Liu, Y.; Qiao, Z. W.; Diestel, L.; Zhou, J.; Huang, A. S.; Caro, J. Polydopamine-based Synthesis of a Zeolite Imidazolate Framework ZIF-100 Membrane with High H_2/CO_2 Selectivity. *J. Mater. Chem. A* **2015**, *3*, 4722−4728.
(45) Smit, B.; Maesen, T. L. M. Molecular Simulations of Zeolites: Adsorption, Diffusion, and Shape Selectivity. *Chem. Rev.* **2008**, *108*, 4125−4184.
(46) Yang, Q. Y.; Liu, D. H.; Zhong, C. L.; Li, J. R. Development of Computational Methodologies for Metal-Organic Frameworks and Their Application in Gas Separations. *Chem. Rev.* **2013**, *113*, 8261−8323.
(47) Watanabe, T.; Sholl, D. S. Accelerating Applications of Metal-Organic Frameworks for Gas Adsorption and Separation by Computational Screening of Materials. *Langmuir* **2012**, *28*, 14114−14128.
(48) Yu, J. M.; Xie, L. H.; Li, J. R.; Ma, Y. G.; Seminario, J. M.; Balbuena, P. CO_2 Capture and Separations using MOFs: Computational and Experimental Studies. *Chem. Rev.* **2017**, *117*, 9674−9754.
(49) Simmons, J. M.; Wu, H.; Zhou, W.; Yildirim, T. Carbon Capture in Metal-Organic Frameworks: Comparative Study. *Energy Environ. Sci.* **2011**, *4*, 2177−2185.
(50) Haldoupis, E.; Nair, S.; Sholl, D. S. Efficient Calculation of Diffusion Limitations in Metal−Organic Framework Materials: A Tool for Identifying Materials for Kinetic Separations. *J. Am. Chem. Soc.* **2010**, *132*, 7528−7539.
(51) Krishna, R.; van Baten, J. M. In Silico Screening of Zeolite Membranes for CO_2 Capture. *J. Membr. Sci.* **2010**, *360*, 323−333.
(52) Wilmer, C. E.; Leaf, M.; Lee, C. Y.; Farha, O. K.; Hauser, B. G.; Hupp, J. T.; Snurr, R. Q. Large-scale Screening of Hypothetical Metal Organic Frameworks. *Nat. Chem.* **2012**, *4*, 83−89.
(53) Chung, Y. G.; Camp, J.; Haranczyk, M.; Sikora, B. J.; Bury, W.; Krungleviciute, V.; Yildirim, T.; Farha, O. K.; Sholl, D. S.; Snurr, R. Q. Computation-ready, Experimental Metal-organic Frameworks: A Tool to Enable High-throughput Screening of Nanoporous Crystals. *Chem. Mater.* **2014**, *26*, 6185−6192.
(54) Gurdal, Y.; Seda, K. A New Approach for Predicting Gas Separation Performances of MOF Membranes. *J. Membr. Sci.* **2016**, *519*, 45−54.
(55) Ahunbay, M. G.; Elliott, J. R.; Talu, O. Surface Resistance to Permeation through the Silicalite Single Crystal Membrane: Variation with Permeant. *J. Phys. Chem. B* **2004**, *108*, 7801−7808.
(56) Newsome, D. A.; Sholl, D. S. Predictive Assessment of Surface Resistances in Zeolite Membranes using Atomically Detailed Models. *J. Phys. Chem. B* **2005**, *109*, 7237−7244.
(57) Newsome, D. A.; Sholl, D. S. Influences of Interfacial Resistances on Gas Transport through Carbon Nanotube Membranes. *Nano Lett.* **2006**, *6*, 2150−2153.
(58) Newsome, D. A.; Sholl, D. S. Atomically Detailed Simulations of Surface Resistances to Transport of CH_4, CF_4, and C_2H_6 through Silicalite Membranes. *Microporous Mesoporous Mater.* **2008**, *107*, 286−295.
(59) Dutta, R. C.; Bhatia, S. K. Interfacial Barriers to Gas Transport in Zeolites: Distinguishing Internal and External Resistances. *Phys. Chem. Chem. Phys.* **2018**, *20*, 26386−26395.
(60) Heffelfinger, G. S.; van Swol, F. Diffusion in Lennard-Jones Fluids using Dual Control Volume Grand Canonical Molecular Dynamics Simulation (DCV-GCMD). *J. Chem. Phys.* **1994**, *100*, 7548−7552.
(61) Xu, L. F.; Sedigh, M. G.; Sahimi, M.; Tsotsis, T. T. Nonequilibrium Molecular Dynamics Simulation of Transport of Gas Mixtures in Nanopores. *Phys. Rev. Lett.* **1998**, *80*, 3511−3514.
(62) Rajabbeigi, N.; Tsotsis, T. T.; Sahimi, M. Molecular Pore-network Model for Nanoporous Materials. II: Application to Transport and Separation of Gaseous Mixtures in Silicon-Carbide Membranes. *J. Membr. Sci.* **2009**, *345*, 323−330.
(63) Naserifar, S.; Tsotsis, T. T.; Goddard, W. A., III; Sahimi, M. Toward a Process-based Molecular Model of SiC Membranes. III: Prediction of Transport and Separation of Binary Gaseous Mixtures based on the Atomistic Reactive Force Field. *J. Membr. Sci.* **2015**, *473*, 85−93.
(64) Botan, A.; Vermorel, R.; Ulm, F. J.; Pellenq, R. J. M. Molecular Simulations of Supercritical Fluid Permeation through Disordered Microporous Carbons. *Langmuir* **2013**, *29*, 9985−9990.
(65) Jin, Z. H.; Firoozabadi, A. Flow of Methane in Shale Nanopores at Low and High Pressure by Molecular Dynamics Simulations. *J. Chem. Phys.* **2015**, *143*, 104315−104327.
(66) Cabrales-Navarro, F. A.; Gómez-Ballesteros, J. L.; Balbuena, P. B. Molecular Dynamics Simulations of Metal-Organic Frameworks as Membranes for Gas Mixtures Separation. *J. Membr. Sci.* **2013**, *428*, 241−250.

https://dx.doi.org/10.1021/acs.jcim.0c00114
J. Chem. Inf. Model. 2020, 60, 2208−2218

(67) Lee, J.; Aluru, N. Water-solubility-driven Separation of Gases using Graphene membrane. *J. Membr. Sci.* **2013**, *428*, 546−553.
(68) Ozcan, A.; Perego, C.; Salvalaglio, M.; Parrinello, M.; Yazaydin, A. O. Concentration Gradient Driven Molecular Dynamics: A New Method for Simulations of Membrane Permeation and Separation. *Chem. Sci.* **2017**, *8*, 3858−3865.
(69) Rajabbeigi, N.; Elyassi, B.; Tsotsis, T. T.; Sahimi, M. Molecular Pore-network Model for Nanoporous Materials. I: Application to Adsorption in Silicon-Carbide Membranes. *J. Membr. Sci.* **2009**, *335*, 5−12.
(70) Pozun, Z. D.; Henkelman, G. A Model to Optimize the Selectivity of Gas Separation in Membranes. *J. Membr. Sci.* **2010**, *364*, 9−16.
(71) Graf, P.; Kurnikova, M. G.; Coalson, R. D.; Nitzan, A. Comparison of Dynamic Lattice Monte Carlo Simulations and the Dielectric Self-energy Poisson-Nernst-Planck Continuum Theory for Model Ion Channels. *J. Phys. Chem. B* **2004**, *108*, 2006−2015.
(72) Boda, D.; Csányi, E.; Gillespie, D.; Kristóf, T. Dynamic Monte Carlo Simulation of Coupled Transport through a Narrow Multiply-occupied Pore. *J. Phys. Chem. C* **2014**, *118*, 700−707.
(73) Seo, Y. G.; Kum, G. H.; Seaton, N. A. Monte Carlo Simulation of Transport Diffusion in Nanoporous Carbon Membranes. *J. Membr. Sci.* **2002**, *195*, 65−73.
(74) Rutkai, G.; Boda, D.; Kristóf, T. Relating Binding Affinity to Dynamical Selectivity from Dynamic Monte Carlo Simulations of a Model Calcium Channel. *J. Phys. Chem. Lett.* **2010**, *1*, 2179−2184.
(75) Ható, Z.; Boda, D.; Kristóf, T. Simulation of Steady-State Diffusion: Driving Force Ensured by Dual Control Volumes or Local Equilibrium Monte Carlo. *J. Chem. Phys.* **2012**, *137*, 054109−054123.
(76) Takaba, H.; Koyama, A.; Nakao, S. Dual Ensemble Monte Carlo Simulation of Pervaporation of an Ethanol/Water Binary Mixture in Silicalite Membrane based on a Lennard−Jones Interaction Model. *J. Phys. Chem. B* **2000**, *104*, 6353−6359.
(77) Rutkai, G.; Kristóf, T. Dynamic Monte Carlo Simulation in Mixtures. *J. Chem. Phys.* **2010**, *132*, 104107−104114.
(78) June, R. L.; Bell, A. T.; Theodorou, D. N. Molecular dynamics study of methane and xenon in silicalite. *J. Phys. Chem.* **1990**, *94*, 8232−8240.
(79) Snurr, R. Q.; June, R. L.; Bell, A. T.; Theodorou, D. N. Molecular simulations of methane adsorption in silicalite. *Mol. Simul.* **1991**, *8*, 73−92.
(80) Zheng, B.; Sant, M.; Demontis, P.; Suffritti, G. B. Force Field for Molecular Dynamics Computations in Flexible ZIF-8 Framework. *J. Phys. Chem. C* **2012**, *116*, 933−938.
(81) Zhang, L. L.; Wu, G.; Jiang, J. W. Adsorption and Diffusion of CO_2 and CH_4 in Zeolitic Imidazolate Framework-8: Effect of Structural Flexibility. *J. Phys. Chem. C* **2014**, *118*, 8788−8794.
(82) McEwen, J.; Hayman, J. D.; Yazaydin, A. O. A Comparative Study of CO_2, CH_4 and N_2 Adsorption in ZIF-8, Zeolite-13X and BPL Activated Carbon. *Chem. Phys.* **2013**, *412*, 72−76.

https://dx.doi.org/10.1021/acs.jcim.0c00114
J. Chem. Inf. Model. 2020, 60, 2208−2218